PAPER

Check for updates

Investigation of dielectric constants of water in a nano-confined pore

Haochen Zhu, [ID] [ab] Fengrui Yang,[ab] Yunjie Zhu,[ab] Aihua Li,[ab] Wenzhi He,[ab] Juwen Huang[ab] and Guangming Li*[ab]

We report the dielectric properties of pure water confined in a silica hydrophilic nanopore determined from the computation of the density of liquid in the confined phase by the grand canonical Monte Carlo (GCMC) simulations. The silica cylindrical nanopore is divided into n concentric radial shells to get a better insight into the dielectric properties of nanoconfined water. We find that the average values of the dielectric constants are very close and almost independent of the number of concentric radial shells. The decrease in the dielectric constant of confined pure water is due to the strong orientation of water dipoles in the vicinity of the surface while water dipoles do not exhibit any preferential orientation in bulk phase.

1. Introduction

Water pollution has attracted more and more people's attention due to the growing population and industrial needs. About one-third of the world's population currently lives now in areas with scarce water resources, and by 2025 this ratio is likely to reach two-thirds.[1,2] Membrane separation technology is a kind of technology which uses selective separation membranes to separate the mixture under external pressure.[3–6] Among which, nanofiltration (NF) membranes have been widely used in drinking water preparation, wastewater treatment, product desalination and purification and other fields due to its excellent separation performance.[7–13] However, due to the special effect brought by the complex structure of nanofiltration membrane, research on the separation mechanism and theoretical model of nanofiltration has become one of the difficulties in the field of nanofiltration research, which limits the development and application of nanofiltration membranes. In recent years the special effect caused by the nanoscale size of nanofiltration membrane has been paid more and more attention.[7–9,14] Among which, dielectric permittivity is the most important one that represents the electrical polarization or the amount of electrical energy stored in a material. The dielectric exclusion is one of the most important separation mechanisms that was firstly considered by Glueckauf[15] and then suggested by Yaroshchuk[16] that the effect of ion interactions with polarization charges or "image forces" at the solution/membrane interface may cause dielectric exclusion. This phenomenon is induced at the solvent-membrane surface because of the

interaction between ions and membrane materials with different dielectric constants. However, the dielectric constant of water in the membrane pore lacks a direct measurement method. The effect of confinement on the dielectric constant is currently a matter of debate in the membrane community and the dielectric constant inside pores of NF membranes is usually used as a fitting parameter.

Molecular dynamics simulation (MD) relies on Newtonian mechanics to simulate the motion of the molecular system, and then extracts samples from the system composed of different states of the molecular system to calculate the configuration integral of the system, and further calculate the thermodynamic quantity and other macroscopic properties of the system based on the results of the configuration integral. It explores the specific behavior of microscopic systems at the molecular level by describing the trajectory of each particle at the atomic level and is widely used in computational chemistry,[17] drug design,[18] computational biology,[19] and materials science.[20]

Since the pore size of nanofiltration membranes is mostly within 1 nm, and the size of water molecules is about 0.3 nm, this means that only 3–4 water molecules can be accommodated in the pore of a nanofiltration membrane. The structure of water molecules under confinement is more orderly than that of bulk space, leading to changes in dielectric constant. The decrease of dielectric constant of the confined phase is caused by the reduction of the rotational freedom of water dipoles near surfaces. Peer's work has shown that water molecules confined in such nanoscale environments exhibit a distinct layered structure inside pores.[21–26] To this end, Varghese *et al.* have found that the rotational diffusion coefficient for water molecules decreased near the solid surface, which is due to the hindered rotation away from the center of the channel to the wall.[22] In addition, Fumagalli *et al.*, probed the dielectric constant of water at nanoscale by applying scanning microscopy

*a*State Key Laboratory of Pollution Control and Resources Reuse, College of Environmental Science and Engineering, Tongji University, 1239 Siping Rd, Shanghai 200092, China. E-mail: ligm@tongji.edu.cn

*b*Shanghai Institute of Pollution Control and Ecological Security, Shanghai 200092, P. R. China

techniques and they found that an extremely low dielectric constant of water in nano-confined surroundings.[26] However, most of these researches have focused on the dielectric constant of water confined in hydrophobic surfaces, few works have investigated the dielectric proprieties of confined water in hydrophilic frameworks. Water layered near hydrophilic surfaces being in proximity of one another can play a role of relatively strong glue between these surfaces. Genko *et al.*, investigated dielectric properties of different hydrophilic/ hydrophobic surfaces and dispersion medium (air, water, chloroform, carbon tetrachloride, and other solvents) using dielectric relaxation spectroscopy and theoretical methods on the interfacial water;[27] Parez *et al.*, compared dielectric properties of water at rutile (hydrophilic) and graphite surfaces (hydrophobic) and they found an augmented density at the rutile surface and an increased molecular polarizability due to the lack of H-bonding partners at the graphite surface.[28] Although the above work investigate the dielectric constant in hydrophilic nanopores, the physical mechanism of dielectric response at the interfaces requires further study and understanding.

In the present work GCMC simulations have been used to investigate dielectric properties of pure water confined in a silica hydrophilic nanopore. Results obtained with the confined nanopore were further discussed by the orientation of water molecules inside the nanopore.

2. Models and computational procedure

The most populated MCM-41 matrix has been applied as the silicate forms by means of the atomic model created by Vink and Barkema.[29] The confined environment of a silica hydrophilic cylindrical nanopore was performed by the procedure of Bródka and Zerda.[30] A cylindrical cavity of 0.6 nm of radius was produced by removing the atoms of silicate matrix. From their coordination numbers, we differentiated bridging oxygens (O_b) bonded to two silicon atoms from nonbridging oxygens (O_{nb}) bonded to only one silicon and bonded to one hydrogen atom (H_{nb}). The nonbridging oxygens were saturated with hydrogen atoms to form surface hydroxyl groups and the density of surface silanol groups is 7.5 nm^{-2} which presented a highly hydrated silica nanopore. Even if the silica matrix remained rigids, we allowed the rotation around the silicon–oxygen (Si–O) bond of the hydroxyl groups from the SHAKE constraints algorithm.[31–34] This process can veritably restore the irregularity of the porous silicate and the interaction between fluid and matrix. The section view of the silica hydrophilic pore is given in Fig. 1.

The total intermolecular potential is composed of a sum of the Lennard-Jones (LJ)[35] and electrostatic interactions (Elec). The most common expressions of the LJ potential are:

$$U_{LJ}(r_{ij}) = \sum_{i<j} 4\varepsilon_{ij}\left[\left(\frac{\sigma_{ij}}{r_{ij}}\right)^{12} - \left(\frac{\sigma_{ij}}{r_{ij}}\right)^{6}\right] \quad (1)$$
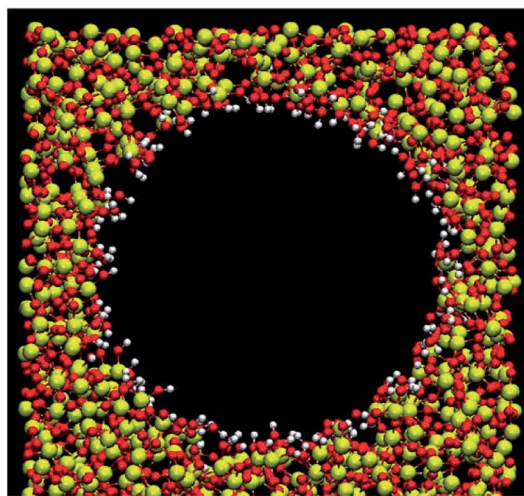

Fig. 1 Section view of the silica hydrophilic pore. Red, white and yellow colors represent the oxygen, hydrogen and silicon atoms, respectively.

where r_{ij} is the distance between the particles, ε_{ij} is the depth of the potential well, σ_{ij} is the cutoff distance between i and j and it gives a measurement of how close two non-bonded particles can get and is thus referred to as the van der Waals radius.

When particles i and j are different chemical species, ε_{ij} and σ_{ij} are usually estimated by the Lorentz–Berthelot (LB) mixing rules,

$$\varepsilon_{ij} = \sqrt{\varepsilon_{ii}\varepsilon_{jj}} \quad (2)$$

$$\sigma_{ij} = \frac{\sigma_{ii} + \sigma_{jj}}{2} \quad (3)$$

The parameters of charges and the Lennard-Jones of silica hydrophilic matrix are given in Table 1. The electrostatic potential is calculated as a sum of interactions between pairs of point charges, using Coulomb's law:

$$U_{Elec} = \sum_{i<j} \frac{q_i q_j}{4\pi\varepsilon_0 r_{ij}} \quad (4)$$

where ε_0 is the vacuum permittivity. However, these forces are a serious problem in computer simulations, since their range is typically greater than half the box length. To handle this problem, the Ewald summation method[36] is applied in our simulation and the electrostatic interaction is described as below:

Table 1 Parameters of charges and the Lennard-Jones of silica hydrophilic matrix. Description of labels given in Fig. 1

	q (e)	σ (Å)	ε (kJ mol^{-1})
H_{nb}	0.206	0.000	0.000
O_b	−0.6349	2.700	1.622
O_{nb}	−0.5399	2.700	1.622
Si	1.2739	0.000	0.000
Si–O	0.320	4.500	0.832

$$U_{\mathrm{Elec}} = \frac{1}{2V_0\varepsilon_0} \sum_{\underline{k}\neq\underline{0}}^{\infty} \frac{\exp(-k^2/4\alpha^2)}{k^2} \left| \sum_{j}^{N} q_j \exp(-i\underline{k}\times\underline{r}_j) \right|^2$$

$$+ \frac{1}{4\pi\varepsilon_0} \sum_{n<j}^{N^*} \frac{q_j q_n}{r_{nj}} \mathrm{erfc}(\alpha r_{nj})$$

$$- \frac{1}{4\pi\varepsilon_0} \sum_{\mathrm{molecules}} \sum_{l\leq m}^{M^*} q_e q_m \left\{ \delta_{lm} \frac{\alpha}{\sqrt{\pi}} + \frac{\mathrm{erf}(\alpha r_{lm})}{r_{lm}^{1-\delta_{lm}}} \right\} \quad (5)$$

where N is the number of ions in the system and N^* the same number discounting any excluded (intramolecular) interactions. M^* represents the number of excluded atoms in a given molecule and includes the atomic self correction. V_0 is the simulation cell volume and $\underline{k}$ is a reciprocal lattice vector defined by $\underline{k} = 2\pi\underline{n}/L^2$, where $\underline{n}$ is the reciprocal space basis vectors, δ_{lm} is the Kronecker delta, erf is the error function, erfc is the complementary error function and α is the convergence parameter (a sharp distribution of charge is set if a large value of α is chosen).

Water molecular model was developed in order to help discovering a adequate structure of water. In this work, we used the non polarizable rigid model TIP4P/2005 formed by Abascal and Vega.[37] In this model, the center of the negative charge corresponding to the oxygen atom is moved along the bisecting line of the H–O–H bond to the position M closer to the hydrogen atom.

In order to simulate realistically the actual process of nanofiltration, the whole system was divided into two parts (see Fig. 2). One was bulk phase which is distributed on both sides of the system and the lengths in x, y and z directions are 35.5 Å, 35.5 Å and 35.5 Å respectively. The solid and adsorbed phases are in the middle of the bulk phase and had a box lengths $L_x = L_y = 35.5$ Å, $L_z = 70$ Å. We formed therefore a rectangular simulation box with $L_x = L_y = 35.5$ Å, and $L_z = 141$ Å. The density of liquid of confined phase was investigated by the grand canonical Monte Carlo (GCMC) and all the simulations were carried out in an efficient isothermal–isosurface–isobaric statistical ensemble[34] with periodic boundary conditions at 298 K and 1 bar. Systems studied

were consisted of 5000 water molecules and performed with the DL_POLY package[38] using the velocity Verlet algorithm[31] and Nose–Hoover thermostat[39] with a time step of 2 fs. The LJ and electrostatic interactions were cut off at 12 Å.

3. Calculations of the dielectric constant

The dielectric constant is defined by the relationship between the polarization and the electric field and it can be determined by the calculations of the dipole moment fluctuations from the fluctuations–dissipation relation[40] as follow:

$$\varepsilon_{\mathrm{b}} = \varepsilon_\infty + \frac{4\pi\left(\langle M^2\rangle - \langle M\rangle^2\right)}{3Vk_{\mathrm{B}}T} \quad (6)$$

where V is the sample volume, $\langle\cdots\rangle$ denotes a statistical average over the different configurations and M is the total dipole moment of the system and obtained by,

$$\vec{M}(t) = \sum_{i=1}^{N_{\mathrm{H_2O}}} \vec{\mu}_i(t) \quad (7)$$

with $\vec{\mu}_i(t)$ the individual molecular dipole moment of the ith water molecule and $N_{\mathrm{H_2O}}$ is the number of water molecules. The term ε_∞ in eqn (6) can be obtained from the Clausius–Mossotti eqn,[41]

$$\frac{\varepsilon_\infty - 1}{\varepsilon_\infty + 2} = \frac{4\pi\alpha}{3\langle v\rangle} \quad (8)$$

where α is the polarizability and v is the molecular volume.

Since we considered a non-polarizable water model throughout this work, $\alpha = 0$ and then eqn (8) leads to $\varepsilon_\infty = 1$. Therefore, for non polarizable solvent molecules eqn (6) takes the form,

$$\varepsilon_{\mathrm{b}} = 1 + \frac{4\pi\left(\langle M^2\rangle - \langle M\rangle^2\right)}{3Vk_{\mathrm{B}}T} \quad (9)$$
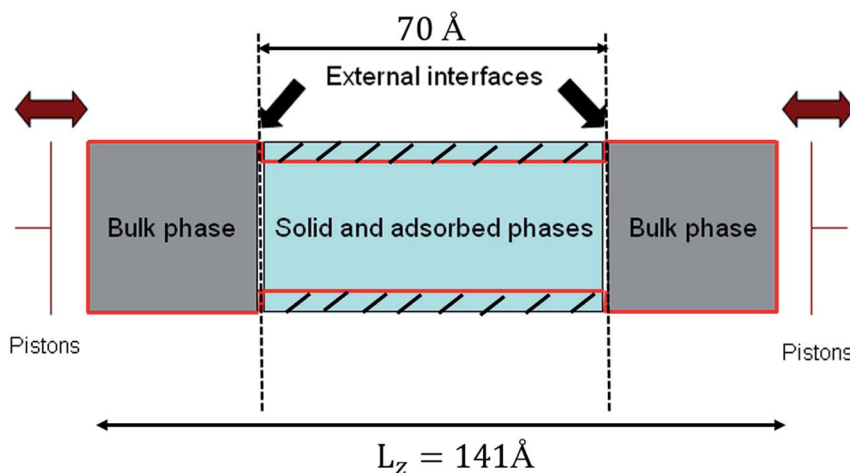

Fig. 2 Schematic of silica hydrophilic pore with two water reservoirs.

For an isotropic medium the ideal limit of zero net dipole moment signifies $M = 0$. ε_b can be calculated from the following relation for sufficiently long simulation,

$$\varepsilon_b = 1 + \frac{4\pi\langle M^2 \rangle}{3Vk_BT} \qquad (10)$$

Throughout this work, eqn (10) was used to compute the dielectric constant of bulk phases. The total dipole moment of a system can be expressed as the integral of the local polarization density $\vec{P}(r)$ over the entire system,[42]

$$\vec{M} = \int \vec{P}(r)\mathrm{d}r \qquad (11)$$

For non-uniform systems, like nanoconfined solutions, a local (*i.e.* space dependent) dielectric constant may be defined. This latter can be computed from dipolar fluctuations within the inhomogeneous fluid that can be characterized by the term $\langle \vec{P}(r) \times \vec{M} \rangle - \langle \vec{P}(r) \rangle \times \langle \vec{M} \rangle$.[40] We used this local approach to compute the dielectric constant of solutions confined inside silica nanopores (ε_p),

$$\varepsilon_p(r) = 1 + \frac{4\pi\left\langle \vec{P}(r) \times \vec{M} \right\rangle - \left\langle \vec{P}(r) \right\rangle \times \left\langle \vec{M} \right\rangle}{3k_BT} \qquad (12)$$

Note that $\vec{P}(r)$ may be replaced by $\vec{M}/V$ in a homogeneous medium.[40] In that case eqn (12) becomes strictly equivalent to eqn (9) and then to eqn (10) for sufficiently long simulation times. We have performed additional calculations (results not shown) to check this point by computing the dielectric constant of water in bulk phase ($\varepsilon_{b,water}$) from the overall (*i.e.* eqn (10)) and the local (*i.e.* eqn (12)) methods. Results show that both methods give identical dielectric constants for simulation times longer than ~3000 ps. In addition, the atoms of the silica material has not accounted for the calculation of the dipolar polarization and dielectric constant.

4. Results and discussion

Fig. 3 shows the radial profile of the dielectric constant of water inside the nanopore ($\varepsilon_{p,water}$).

In order to have a deep understanding of the dielectric properties in nanoconfined water, we divided the silica cylindrical nanopore into n concentric radial shells as shown in inset of Fig. 3. The dielectric constant of confined pure water has been computed by applying eqn (12) in each concentric shell for various values of n. Results are shown in Fig. 3 for $n = 10$, 20, 50 and 200. Although some discrepancies appear locally, the average values of the dielectric constants are very close and almost independent of the number of concentric radial shells, at least up to $n = 50$ (see Table 2). For very large values of n, strong fluctuations appear in the dielectric constant profile (see *e.g.* $n = 200$ in Fig. 3) and a variation of the average dielectric constant of about 10% (see Table 2) is observed. Gereben and Pusztai have pointed out that the static dielectric constant computed from MD simulations may depend on the size of the system (*i.e.* the number of water molecules in the simulation).[43] These authors found a variation of the dielectric constant of

Table 2 Radially averaged dielectric constant of confined water computed by dividing the pore into n concentric shells

n	10	20	50	200
$\varepsilon_{p,water}$ (average value)	25.5	25.4	25.5	23.2

Fig. 3 Radial profile of the dielectric constant of water inside nanopore ($\varepsilon_{p,water}$) computed by dividing the pore into various numbers of concentric shells (n).
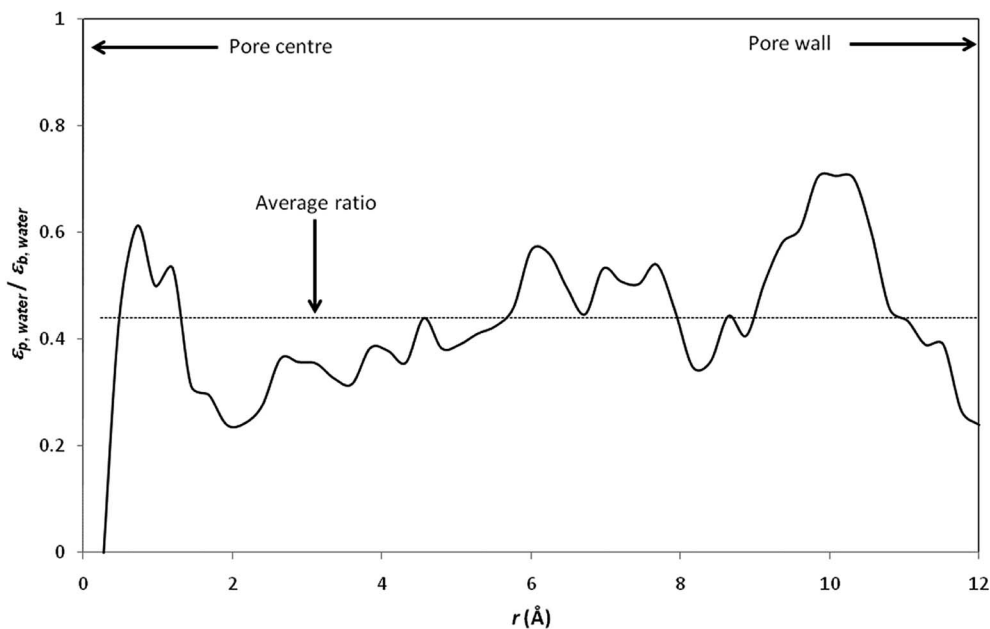
Fig. 4 Ratio between the dielectric proprieties of confined water ($\varepsilon_{p,water}$) and the dielectric proprieties of bulk water ($\varepsilon_{b,water}$). The local dielectric constant inside the nanopore was computed by dividing the nanopore into 50 concentric radial shells (*i.e.* $n = 50$ in inset of Fig. 3).

about 10% when considering systems ranging from 216 to 16 000 polarizable water molecules and a non-monotonous variation of the dielectric constant with the system size. This is likely to affect our results since the number of water molecules within the n concentric shells (see inset of Fig. 3) differ from one shell to another.

When n is too large, the number of water molecules in each layer is quite low and statistical uncertainties on the fluctuation term on the right hand side of eqn (12) are dramatically amplified, which can even lead to nonphysical negative values as shown in Fig. 3 This might be an additional difficulty for the determination of dielectric constants inside pores of realistic nanoporous membranes whose effective diameters are expected to be 2–3 times smaller than that of our model nanopore.

Fig. 4 shows the radial variation of the ratio between the dielectric constant of confined water ($\varepsilon_{p,water}$) and the dielectric constant of bulk water ($\varepsilon_{b,water}$). The dielectric constant of pure water is found to be reduced by a factor of more than 2 with respect to its bulk value (the average $\varepsilon_{p,water}/\varepsilon_{b,water}$ ratio was found to be 0.44; note that values obtained at the pore centre should not be considered because the analysis is biased by the low statistics resulting from the small number of water molecules inside the central cylindrical shell).

It should be stressed that the ratio $\varepsilon_{p,water}/\varepsilon_{b,water}$ inferred from our simulations is significantly lower than that obtained by Senapati and Chandra for spherical cavities of 24.4 Å in diameter.[21] Indeed, these authors obtained $\varepsilon_{p,water}/\varepsilon_{b,water}$ ratios of 0.88 and 0.83 with SSD and SPC/E water models, respectively. Of course, the different geometries considered in Senapati and Chandra's work and in the present work make difficult a direct comparison between our results. Nevertheless, it should be noted that a recent MD study performed by Gereben and Pusztai has

clearly shown that trajectories recorded for times shorter than 5–6 ns are not applicable for providing a good estimate of the dielectric constant.[43] Unfortunately, Senapati and Chandra reported MD simulations performed over simulation times shorter than 2 ns including equilibration time. On the other hand, we performed data analysis of dielectric constants inside pore for the last 2 ns of our simulations, after 4–7 ns of equilibration, which means that our total simulation times were 7–10 ns.

In an attempt to understand the origin of the decrease in the dielectric constant of confined pure water we focused on the orientation of water molecules inside the nanopore. We define θ
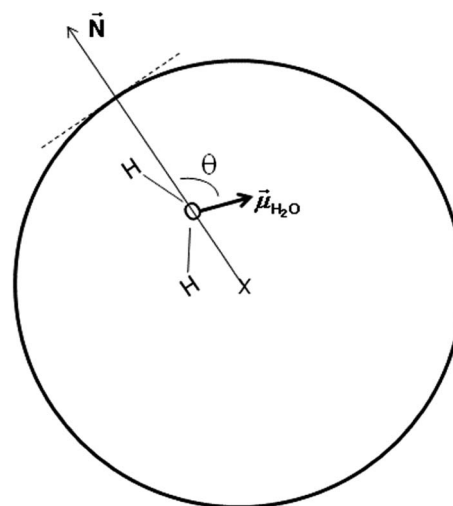

Fig. 5 Schematic representation of the angle θ between the water dipole moment and the vector normal to the pore surface and connecting the pore center and the center of mass of the oxygen atom of the water molecule.
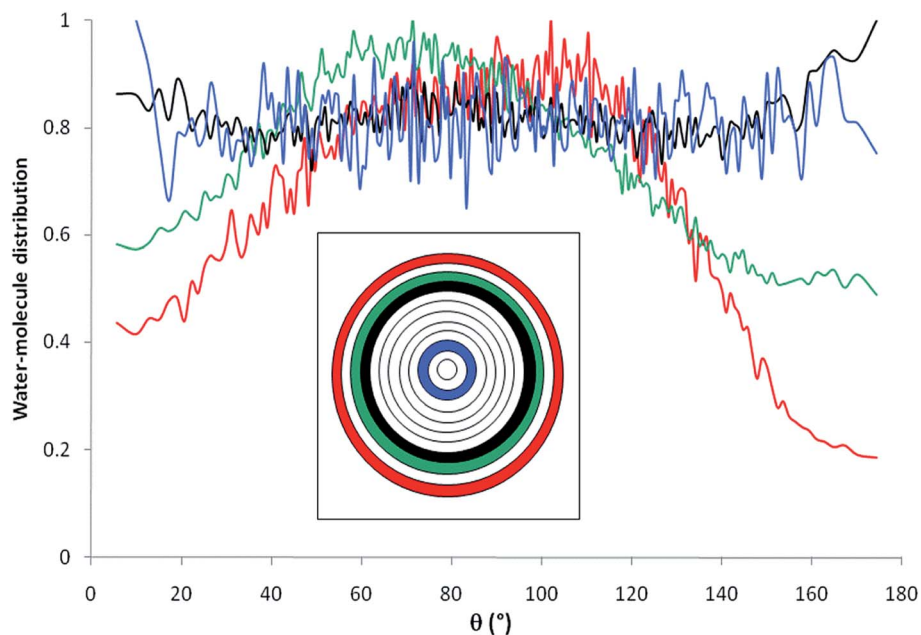
Fig. 6 Water molecules orientations inside the nanopore (filled with pure water); θ represents the angle composed by the water dipole moment and the normal vector. The inset shows the location of the different layers inside the pore ($n = 12$).

as the angle between the dipole moment of a water molecule ($\vec{\mu}_{H_2O}$) and the vector normal to the pore surface ($\vec{N}$) which connects the pore center and the center of mass of the oxygen atom of the water molecule (see Fig. 5).

Fig. 6 shows the distribution of water molecules inside the nanopore as a function of θ. The pore was divided into concentric shells of thickness 1 Å (*i.e.* $n = 12$, see inset in Fig. 3). Water molecules located within the first three shells in the vicinity of the pore surface (that is the first hydration layer) exhibit preferential orientation with $\theta \sim 90–100°$ while molecules located farther from the surface do not align their dipole

according to a preferential orientation with respect to the pore surface. This strong orientation of water dipoles in the vicinity of the surface may explain the decrease in the dielectric constant of pure water under confinement with respect to the bulk phase where water dipoles do not exhibit any preferential orientation. This decrease of dielectric constant was due to the fact that hydrogen bond (HB) rearrangement of water molecules was limited and led to a decrease in the fluctuations of water dipoles. In the first three shells that are closer to the interface, the preferred dipole orientation is a slight tilt toward the interface. This tilt is more pronounced closer to the interface.
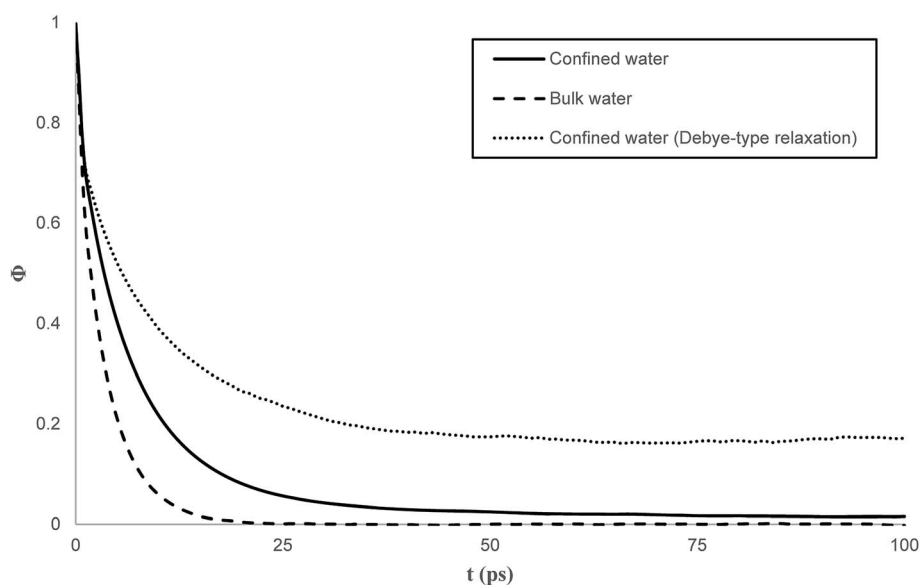

Fig. 7 Self time correlation function of the dipole moments for bulk and confined water.
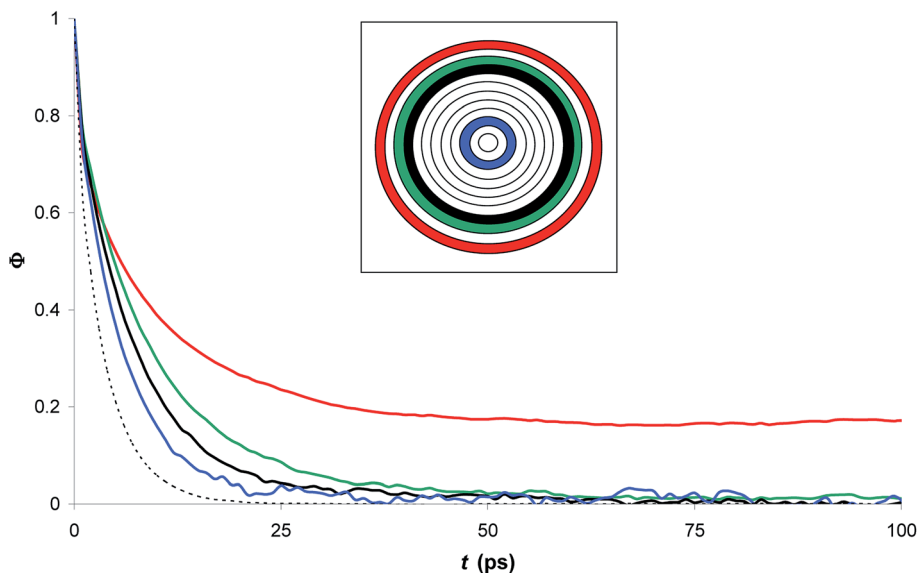
Fig. 8 Time correlation function of the dipole moments in different zones inside the nanopore (filled with pure water). The inset shows the location of the different layers inside the pore ($n = 12$); dotted line: bulk water.

This behavior is consistent with water molecules participating in some H-bonds with interfacial oxygens and hydrogens, in addition to the water–water H-bonds.

Another important parameter of dielectric properties is the so-called dielectric relaxation time of polar fluids, τ_{rel}, given by assuming a Debye exponential behavior of self-correlation function of dipole moments:[44]

$$\Phi(t) = \exp(-t/\tau_{rel}) \tag{13}$$

where $\Phi(t)$ is the self-correlation function of dipole moments and determined as:

$$\Phi(t) = \frac{\left\langle \overrightarrow{\mu}(t) \times \overrightarrow{\mu}(0) \right\rangle}{\left\langle \overrightarrow{\mu}(0)^2 \right\rangle} \tag{14}$$

Fig. 7 compares the time correlation function of the dipole moments of pure water in bulk and confined phases respectively. It is clearly seen that dipole moments relax much faster in bulk phase than that of confined phase. The dynamical dielectric properties of water molecules can be performed *via* the correlation time of dipole moments, τ, computed as,[45]

$$\tau = \int_0^\infty \Phi(t) \mathrm{d}t \tag{15}$$

In bulk phase, the correlation time of dipole moments of water in Fig. 7 was taken into account in eqn (13) and (15) and we obtained $\tau = 3.9$ ps and $\tau_{rel} = 3.1$ ps. The rather small difference between τ and τ_{rel} indicates that the behavior of bulk water is close to that of a Debye dielectric.

Interestingly, the correlation time of the moment dipoles rises to 16.7 ps inside the nanopore, which indicates that dipole moments remain oriented along fixed directions for much longer times than in bulk phase. Furthermore, the relaxation time τ_{rel}

determined from eqn (13) is found to be 6.2 ps. Although the analysis of τ and τ_{rel} lead to a similar qualitative conclusion, *i.e.* water molecules relax much slower inside the nanopore than in the bulk phase, it can be noted that the large discrepancy between τ and τ_{rel} observed for confined water molecules indicate a different relaxation mode under nanoconfinement and confined water does not exhibit a Debye-type relaxation with a single relaxation time anymore. To get further insight in the dielectric properties of confined water we computed the time correlation function of the dipole moments in different areas inside the nanopore. Results are shown in Fig. 8 which clearly puts in evidence a distribution of the correlation times inside the nanopore with a delayed relaxation with respect to the bulk phase (see dotted line in Fig. 8) and a monotonous increase in the relaxation time when water molecules approach the pore surface (in the first interfacial shell we found $\tau > 200$ ps from eqn (11)). This indicates a decrease in the rotational dynamics of water dipoles close to the pore surface.

Finally, it is interesting to note that although both the water density and the orientation of water dipoles (see Fig. 5) are bulk-like in the central part of the nanopore, the dielectric properties remain significantly affected by confinement.

5. Conclusion

In this work the computation of the density of liquid in a silica hydrophilic nanopore was executed by the grand canonical Monte Carlo (GCMC) and all the simulations were carried out in an efficient isothermal–isosurface–isobaric statistical ensemble. The local dielectric constants were computed from dipolar fluctuations within the inhomogeneous fluid. For very large values of concentric shells (n), strong fluctuations appear in the dielectric constant profile and a variation of the average dielectric constant of about 10% is observed. The dielectric constant of pure water was found to be reduced by a factor of

more than 2 with respect to its bulk value (the average $\varepsilon_{\text{p,water}}/\varepsilon_{\text{b,water}}$ ratio was found to be 0.44). That was imputed to water molecules located within the first three shells in the vicinity of the pore surface which exhibit preferential orientation with $\theta \sim 90\text{–}100°$ in nanoconfined phase. Regarding the correlation time of the moment dipoles we observed that dipole moments remained oriented along fixed directions for much longer times than in bulk phase and the correlation times inside the nanopore had a delayed relaxation with respect to the bulk phase.

Conflicts of interest

There are no conflicts to declare.

Acknowledgements

References

1 I. A. Wright, S. Wright, K. Graham and S. Burgin, *Land Use Policy*, 2011, **28**, 353–360.

2 V. Kumar, R. D. Parihar, A. Sharma, P. Bakshi, G. P. Singh Sidhu, A. S. Bali, I. Karaouzas, R. Bhardwaj, A. K. Thukral, Y. Gyasi-Agyei and J. Rodrigo-Comino, *Chemosphere*, 2019, **236**, 124364.

3 S. Alzahrani and A. W. Mohammad, *Journal of Water Process Engineering*, 2014, **4**, 107–133.

4 P. Pal, in *Industrial Water Treatment Process Technology*, ed. P. Pal, Butterworth-Heinemann, 2017, pp. 173–242, DOI: 10.1016/b978-0-12-810391-3.00005-9.

5 W. R. Bowen, A. W. Mohammad and N. Hilal, *J. Membr. Sci.*, 1997, **126**, 91–105.

6 J. R. Werber, A. Deshmukh and M. Elimelech, *Environ. Sci. Technol. Lett.*, 2016, **3**, 112–120.

7 A. Szymczyk and P. Fievet, *J. Membr. Sci.*, 2005, **252**, 77–88.

8 A. Yaroshchuk, M. L. Bruening and E. Zholkovskiy, *Adv. Colloid Interface Sci.*, 2019, **268**, 39–63.

9 B. Balannec, A. Ghoufi and A. Szymczyk, *J. Membr. Sci.*, 2018, **552**, 336–340.

10 H. Zhu, A. Szymczyk and B. Balannec, *J. Membr. Sci.*, 2011, **379**, 215–223.

11 P. Ortiz-Albo, R. Ibanez, A. Urtiaga and I. Ortiz, *Sep. Purif. Technol.*, 2019, **210**, 746–753.

12 K. Jiang, H. Kuang, T. Qin, M. Song, J. Zhou, P. Yang, W. Zhuang, H. Ying and J. Wu, *RSC Adv.*, 2018, **8**, 12672–12683.

13 O. Labban, C. Liu, T. H. Chong and J. H. Lienhard, *J. Membr. Sci.*, 2018, **554**, 26–38.

14 CN107096401-A.

15 E. Glueckauf, *Nature*, 1966, **211**, 1227–1230.

16 A. E. Yaroshchuk, *Adv. Colloid Interface Sci.*, 2000, **85**, 193–230.

17 R. Sardella, E. Camaioni, A. Macchiarulo, A. Gioiello, M. Marinozzi and A. Carotti, *TrAC, Trends Anal. Chem.*, 2020, **122**, 115703.

18 Z. Shariatinia and A. Mazloom-Jalali, *J. Mol. Liq.*, 2019, **273**, 346–367.

19 M. Arnittali, A. N. Rissanou and V. Harmandaris, *Procedia Computer Science*, 2019, **156**, 69–78.

20 X. Liu, T. Wang and M. He, *J. Mol. Liq.*, 2019, **288**, 111034.

21 S. Senapati and A. Chandra, *J. Phys. Chem. B*, 2001, **105**, 5106–5109.

22 S. Varghese, S. K. Kannam, J. S. Hansen and S. P. Sathian, *Langmuir*, 2019, **35**, 8159–8166.

23 C. Zhang, F. Gygi and G. Galli, *J. Phys. Chem. Lett.*, 2013, **4**, 2477–2481.

24 J. N. Israelachvili and R. M. Pashley, *Nature*, 1983, **306**, 249–250.

25 M. F. Toney, J. N. Howard, J. Richer, G. L. Borges, J. G. Gordon, O. R. Melroy, D. G. Wiesler, D. Yee and L. B. Sorensen, *Nature*, 1994, **368**, 444–446.

26 L. Fumagalli, A. Esfandiar, R. Fabregas, S. Hu, P. Ares, A. Janardanan, Q. Yang, B. Radha, T. Taniguchi, K. Watanabe, G. Gomila, K. S. Novoselov and A. K. Geim, *Science*, 2018, **360**, 1339.

27 V. M. Gun'ko, V. V. Turov, V. M. Bogatyrev, V. I. Zarko, R. Leboda, E. V. Goncharuk, A. A. Novza, A. V. Turov and A. A. Chuiko, *Adv. Colloid Interface Sci.*, 2005, **118**, 125–172.

28 S. Parez, M. Předota and M. Machesky, *J. Phys. Chem. C*, 2014, **118**, 4818–4834.

29 R. L. C. Vink and G. T. Barkema, *Phys. Rev. B: Condens. Matter Mater. Phys.*, 2003, **67**, 245201.

30 A. Bródka and T. W. Zerda, *J. Chem. Phys.*, 1996, **104**, 6319–6326.

31 M. Allen and D. Tildesley, *Computer simulation of liquids*, Oxford, New York, 1989, p. 385.

32 J.-P. Ryckaert, G. Ciccotti and H. J. Berendsen, *J. Comput. Phys.*, 1977, **23**, 327–341.

33 A. Ghoufi, D. Morineau, R. Lefort and P. Malfreyt, *J. Chem. Theory Comput.*, 2010, **6**, 3212–3222.

34 A. Ghoufi, D. Morineau, R. Lefort, I. Hureau, L. Hennous, H. Zhu, A. Szymczyk, P. Malfreyt and G. Maurin, *J. Chem. Phys.*, 2011, **134**, 074104.

35 J. E. Lennard-Jones, *Proc. R. Soc. A*, 1924, **106**, 463–477.

36 P. Ewald, *Ann. Phys.*, 1921, **64**, 253–287.

37 J. L. Abascal and C. Vega, *J. Chem. Phys.*, 2005, **123**, 234505.

38 W. Smith and T. Forester, *J. Mol. Graphics*, 1996, **14**, 136–141.

39 D. J. Evans and B. L. Holian, *J. Chem. Phys.*, 1985, **83**, 4069–4074.

40 V. Ballenegger and J.-P. Hansen, *J. Chem. Phys.*, 2005, **122**, 114711.

41 G. Lamoureux, A. D. MacKerell and B. Roux, *J. Chem. Phys.*, 2003, **119**, 5185–5197.

42 H. A. Stern and S. E. Feller, *J. Chem. Phys.*, 2003, **118**, 3401–3412.

43 O. Gereben and L. Pusztai, *Chem. Phys. Lett.*, 2011, **507**, 80–83.

44 J. Martí, E. Guàrdia and J. A. Padró, *J. Chem. Phys.*, 1994, **101**, 10883–10891.

45 M. Neumann, *J. Chem. Phys.*, 1986, **85**, 1567–1580.